Supplementary Information

S1 Transformation of the payoff matrix as it relates to the game space

The dynamics in a two-player game are often displayed as quadrants in a 2D "game space" with quadrants corresponding to different dynamical outcomes (**Fig. 5A**) [1]. Our variable transformation of the payoff matrix allows us to highlight how the quadrants are regions defined by interaction strengths relative to intrinsic selection and their analytical forms. In the intrinsic and extrinsic form of the payoff matrix, these axes correspond to $(g_m + \beta_{mw} - g_w)$ and $(g_w + \beta_{wm} - g_m)$. Here g_i is the intrinsic growth rate of type i and β_{ij} is the maximum extent to which interaction with type j affects the growth of i. In this transformed basis we can also write these as $g_w(\alpha_{mw} - s_m)$ and $g_w(s_m + \alpha_{wm})$ where $a = g_w$ and the quadrants can be defined by conditions on α_{mw} and α_{wm} relative to the homogeneous mutant population selection coefficient s_m (**Fig. 5B**). For the novel "interaction-selection" plot (**Fig. 5C**), we can plot the selection normalized interaction coefficients (α_{ij}/s_i, α_{ji}/s_i). As we move through different values of α_{wm} and α_{mw} relative to s_m the resultant equilibrium state is modified. We highlight the unit circle in this plot as a key region where intrinsic selection differences are dominant. As might be expected, within this circle, the game dynamics of the system, dominated by intrinsic selection, will align with the quadrant representing dominance by the same population. Deterministic boundaries between the universality classes in all phase spaces occur along the lines $\alpha_{wm} = -s_m$ and $\alpha_{mw} = s_m$ For example, the cooperation quadrant (top right) is defined by $\alpha_{wm} > s_m$ and $\alpha_{mw} > -s_m$.

S2 Derivation of deterministic frequency-dependent selection coefficient

To derive the frequency-dependent selection coefficient for our deterministic model we use the payoff matrix and fitness vector to calculate the selection coefficient. Our decomposition of the payoff matrix into selection and interaction components results in the following fitness vector:

$$\begin{aligned}\vec{\phi}(\vec{x}) &= P \cdot \vec{x} \\ &= \begin{pmatrix} 1 & 1+\alpha_{wm} \\ 1+s_m+\alpha_{mw} & 1+s_m \end{pmatrix} \begin{pmatrix} x \\ 1-x \end{pmatrix} \\ &= \begin{pmatrix} 1+\alpha_{wm}x \\ 1+s_m+\alpha_{mw}(1-x) \end{pmatrix}\end{aligned} \tag{S1}$$

where $\vec{x} = (1-x, x)$ is the vector of frequencies of the wild-type and the mutant. The first component of $\vec{\phi}(\vec{x}) = (\phi_w(\vec{x}), \phi_m(\vec{x}))$ is the wild-type fitness $\phi_w(\vec{x})$, and the second component is the mutant fitness $\phi_m(\vec{x})$. The frequency-dependent selection coefficient $\sigma_m(\vec{x})$ that is to replace the constant selection coefficient s_m is defined by the ratio of frequency-dependent fitnesses, minus 1:

$$\begin{aligned}\sigma_m(x) &:= \frac{\phi_m(\vec{x})}{\phi_w(\vec{x})} - 1 \\ &= \frac{1+s_m+\alpha_{mw}(1-x)}{1+\alpha_{wm}x} - 1 = \frac{s_m + \alpha_{mw} - (\alpha_{wm}+\alpha_{mw})x}{1+\alpha_{wm}x}.\end{aligned} \tag{S2}$$

S3 Deterministic Regime Derivations

The regimes can be defined by the selection coefficient or the stationary solution(s). We use our reformulation to produce the following derivations for maintenance, mirroring, masking, and mimicry.

Regimes by dynamics

Our four regimes correspond to equivalence of the frequency-dependent selection to a specific value of frequency-independent selection. Given that the selection coefficient determines the evolutionary dynamics, the regimes are also defined by equivalent *dynamics* when the frequency-dependent selection coefficient is equal to the following reference values:

Maintenance

$$
\begin{aligned}
\sigma_m(x) &= s_m \\
\frac{1+s_m+\alpha_{mw}(1-x)}{1+\alpha_{wm}x} - 1 &= s_m \\
\frac{1+s_m+\alpha_{mw}(1-x)}{1+\alpha_{wm}x} &= 1+s_m \\
1+s_m+\alpha_{mw}(1-x) &= (1+s_m)(1+\alpha_{wm}x) \\
\rightarrow \alpha_{mw} &= \alpha_{wm} = 0
\end{aligned}
\tag{S3}
$$

Mirroring

$$
\begin{aligned}
\sigma_m(x) &= -s_m \\
\frac{1+s_m+\alpha_{mw}(1-x)}{1+\alpha_{wm}x} - 1 &= -s_m \\
\frac{1+s_m+\alpha_{mw}(1-x)}{1+\alpha_{wm}x} &= 1-s_m \\
1+s_m+\alpha_{mw}(1-x) &= (1-s_m)(1+\alpha_{wm}x) \\
\rightarrow \alpha_{mw} &= -2s_m, \alpha_{wm} = 2s_m/(1-s_m)
\end{aligned}
\tag{S4}
$$

Masking

$$
\begin{aligned}
\sigma_m(x) = 0 \frac{1+s_m+\alpha_{mw}(1-x)}{1+\alpha_{wm}x} - 1 &= 0 \\
\frac{1+s_m+\alpha_{mw}(1-x)}{1+\alpha_{wm}x} &= 1 \\
1+s_m+\alpha_{mw}(1-x) &= 1+\alpha_{wm}x \\
\rightarrow \alpha_{mw} &= -s_m, \alpha_{wm} = s_m
\end{aligned}
\tag{S5}
$$

Mimicry

$$
\begin{aligned}
\frac{1+s_m+\alpha_{mw}(1-x)}{1+\alpha_{wm}x} - 1 &= s' \\
\frac{1+\alpha_{mw}(1-x)}{1+\alpha_{wm}x} &= 1+s' \\
1+\alpha_{mw}(1-x) &= (1+\alpha_{wm}x)(1+s) \\
\rightarrow \alpha_{mw} &= s', \alpha_{wm} = -s'(1+s')
\end{aligned}
\tag{S6}
$$

Regimes by steady state only

The deterministic replicator equation describing population fraction has 2 or 3 solutions (proportion x_∞, of varying stability). The solutions to the replicator equation (**Eq.** (B2)), correspond to deterministic steady states of the allele fraction, x, denoted x_∞. However, for the non-interacting ($\alpha_{wm}, \alpha_{mw} = 0$), non-mutating system, there are two fixed points, $x_\infty = 0$ and $x_\infty = 1$, where the stability depends on the sign of s_m. There is an additional equilibrium solution x_∞^{int} in the presence of interactions,

$$
x_\infty = 0, x_\infty = 1, x_\infty^{int} = \frac{\alpha_{mw}+s_m}{\alpha_{mw}+\alpha_{wm}} \text{ where } \alpha_{mw}+\alpha_{wm} \neq 0,
\tag{S7}
$$

Thus, the additional equilibrium solution x_∞^{int} in the presence of interactions is *indistinguishable* from possible outcomes of the non-interacting system when $x_\infty^{int} = 0$ or $x_\infty^{int} = 1$. For these steady-state solutions for, the interaction coefficients are partially constrained,

$$
\begin{aligned}
&x_\infty^{int} = 0 \rightarrow \alpha_{mw} = -s_m \text{ and } \alpha_{mw} \neq -\alpha_{wm} \\
&x_\infty^{int} = 1 \rightarrow s_m = \alpha_{wm} \text{ and } \alpha_{mw} \neq -\alpha_{wm}.
\end{aligned}
\tag{S8}
$$

S4 Stochastic steady-state solution can be expressed in terms of interaction strengths

A form of steady-state solution $\rho^{\mathrm{eq}}(x)$ for the Fokker-Planck equation in **Eq.** (B**3**) is

$$\rho^{\mathrm{eq}}(x) = C\big[\exp\big(-U(x)\big)\big], \tag{S9}$$

where C is a normalization constant, and $U(x) = \ln D(x) - \int_0^x dx'\, v(x')/D(x')$. For our interacting model, the integral can be carried out explicitly, yielding

$$U(x) = (1-2N\mu)\ln(x(1-x)) - 2N\left[\frac{(1+s_m)\alpha_{wm}+(1+\alpha_{wm})\alpha_{mw}}{\alpha_{wm}^2}\ln(1+\alpha_{wm}x) - \frac{\alpha_{wm}+\alpha_{mw}}{\alpha_{wm}}x\right] - \ln(2N). \tag{S10}$$

Our solution describes a probability density function (PDF) for a given population size, mutation rate, selection coefficient, and interaction terms. The steady-state solution for the PDF describes the probability distribution of a given mutant fraction x at equilibrium for given parameters. Knowledge of $\rho^{\mathrm{eq}}(x)$ can then be used to calculate summary values of the distribution, for example, the modal mutant population fraction using or the mean $\bar{x} = \int_0^1 dx' x' \rho^{\mathrm{eq}}(x')$. We show (**Fig. S1**) that the game landscape is populated by probability density functions approximating the outcomes of the deterministic system, including bimodal distributions.

We observe (**Fig S3**) that under very small ecological interaction and at low mutation rates, the form of the solution is similar to the deterministic case in the absence of noise, where the distributions approach delta functions at either $x = 0$ or $x = 1$. The values of α_{mw}, α_{wm}, and μN alter the width of the peaks in the probability distributions.

S5 Relationship between interaction coefficients

In the main text, we show the frequency-dependent selection coefficient for the stochastic system ($\sigma(x_{mode})$) can be expressed as a function of the interaction coefficients. We rearrange that expression to produce an equation for one interaction coefficient at generic selection coefficient $\sigma(x_{mode})$. We replace $\sigma(x_{mode})$ with σ for brevity. This relationship between the interaction coefficients and intrinsic selection coefficient is as follows:

$$\alpha_{wm} = \frac{2s_m(s_m-\sigma) + (s_m + 2\mu - \sqrt{4\mu^2+s_m^2})\alpha_{mw}}{(1+\sigma)(s_m - 2\mu + \sqrt{4\mu^2+s_m^2})}. \tag{S11}$$

Plots of these relationships are shown in Figure S5.

S6 Agreement of analytics with stochastic simulations across selection and interaction strengths

Where the outcomes of deterministic games are redundant in their contributing game interactions, the stochastic Fokker-Planck system produces a probability distribution dependent on N,μ,s,a_{mw}, and a_{wm}. By simulating stochastic population dynamics, we can sample populations to create a probability distribution over the fractions of mutant and wild-type alleles.

The mean value of the simulation fractions is plotted in **Figure S1** for a specific $s_m(= 0.05)$ with varying interaction coefficients, and the corresponding theoretical probability distributions in several cases are shown for comparison. It is worth noting that the "snowdrift" game from the lower left quadrant in traditional game space ($c < a$ and $b < d$) has two peaks in its stationary Fokker-Planck solution, and the height of these peaks becomes more uneven with distance away from the line $\alpha_{wm} = \alpha_{mw} - 2s_m$. The width of the peaks in all sections increases with mutation rate μ.

In the Wright-Fisher model, with mutation and strong selection, a population will move to the peak of the landscape in a single-peaked landscape, whereas in a flat landscape, fluctuates stochastically around equal proportions of all genotypes. Without interactions, the results of the Wright-Fisher model depend only on the intrinsic (genetic) fitness landscape, in particular, whether the landscape is neutral or peaked, and the mutation rate. To validate the predicted result of interactions in evolutionary simulation models we added randomly distributed interaction strengths to a Wright-Fisher model of both single-peaked ($s_m ! = 0$) and flat ($s_m = 0$) landscapes.

In **Figure S2** and **Figure S4** we examine the interaction population's probability density function for the stationary solution. In **Figure S2A** we plot the modal values of the analytical solution over varying α_{mw} and α_{wm} for a given selection and mutation space. To validate these distributions we sampled the frequency spectrum of the population in simulations at long time points (between 100 and 10,000 generations). We compared this frequency distribution to our analytical probability density

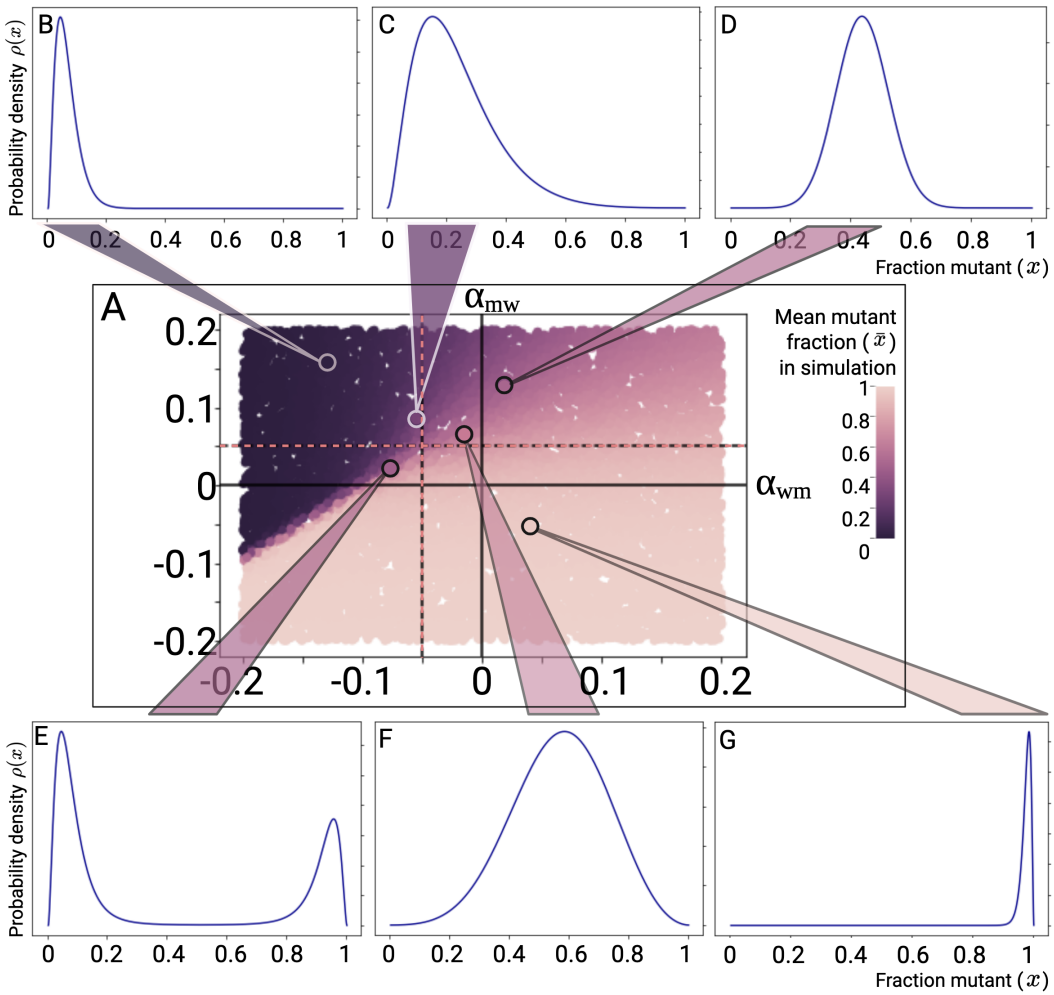

Figure S1. **Simulations and equivalent Fokker-Planck solutions for examples of a stochastic evolving and mutating population.** **(A)**The central plot displays the mean fraction of the mutant population ($\bar{x}$), plotted for 10,000 randomly distributed game parameters. Mean mutant fractions are plotted against randomly sampled interaction strengths, with mutant selection advantage $s_m = 0.05$, $N = 1000$, $\mu = 0.005$. The average (mean) proportion of mutant was plotted for each pair of interaction coefficients. Simulation results are colored by population fraction, with 100% wild-type, 0% mutant in dark purple, and 100% mutant, 0% wild-type population in cream. 10,000 random values of α_{mw}, α_{wm} in the interval $[-0.2, 0, 2]$ were sampled to populate the phase plot. Six distributed examples (**B-G**) of the analytical Fokker-Planck equilibrium solution for $\rho(x)$ against x are shown and their approximate position in the simulation space is highlighted. Distributions from the upper left and lower right (e.g., **B**, **G**) have distributions strongly peaked near 0% and 100% mutant fractions, respectively. The upper right quadrant (e.g., **D**, **F**) shows stable co-existence, with solutions and simulations in the bottom left quadrant (e.g., **E**) representing probability distributions with two peaks, one at 100% wild-type and one at 0% wild-type.

equilibrium solution for the Fokker-Planck equation with interactions. In the case of $s_m = 0$, we regain the four-quadrant game plot, representing the different classical games and their outcomes.

The equilibrium distribution of a system with known monoculture fitnesses and no game interactions is well defined and understood in population genetics. As a result, the equilibrium distributions/evolutionary outcomes measured in experiments are often assumed to result from entirely intrinsic fitness differences. This assumption does not account for potential interactions between populations. As seen in **Figure 2**, the survival of the fittest (under which the 'fittest' genotype prevails), can result in multiple populations co-occurring and becomes population and interaction-dependent.

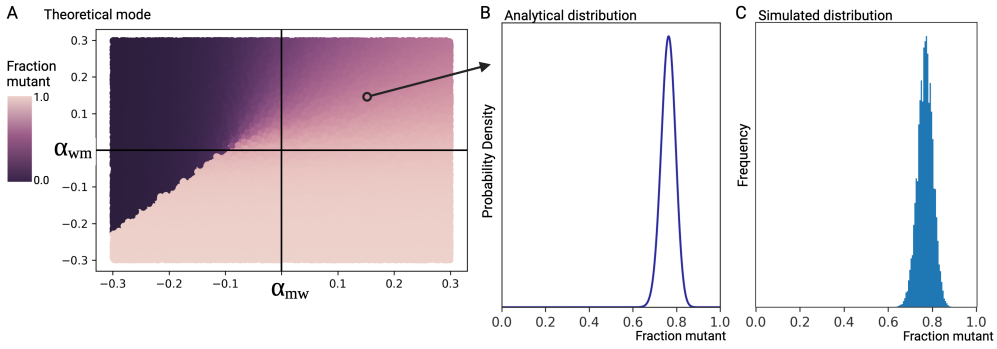

Figure S2. Fokker-Planck (FP) distribution compared to stochastic simulation results. (A) The modal value of the analytical FP distribution is plotted for 100,000 randomly generated pairs of interaction terms. Modal values of 100% wild-type are dark purple and 100% mutant fraction are colored cream. **(B)** We highlight the shape of the analytical probability density distribution in a specific Fokker-Planck solution ($\alpha_{wm} = 0.16$, $\alpha_{mw} = 0.14$, $s_m = 0.1$) and compare theoretical results in plot **(B)** to simulation. **(C)** Distribution of sampled fractions between 200 to 500 generations in 500 independent simulations is shown. These simulations had a selection coefficient of $s_m = 0.1$, representing a fitter mutant population. The histogram is a sampled distribution of the population fraction, with each sample measured at $t > 200$ generations from 500 simulations under these conditions. Further examples are shown in **Figure S4**.

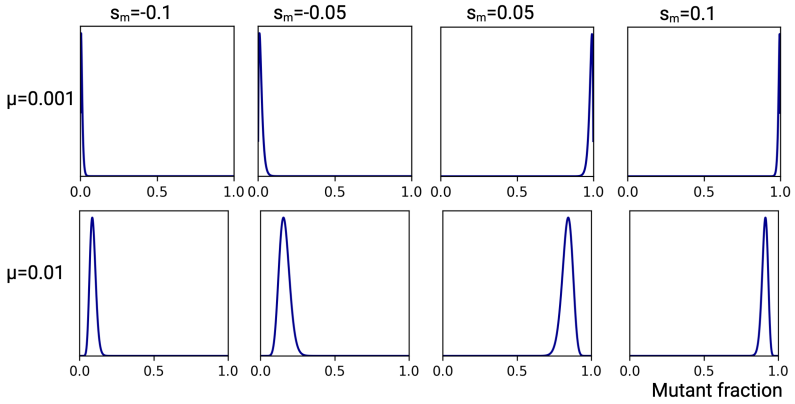

Figure S3. Fokker-Planck analytical probability density distribution for minimal interaction strengths agrees with baseline expectations. Each example represents the analytical distribution for a given population size (N=1000) and given small interaction strengths ($\alpha_{wm} = \alpha_{mw} = 0.0001$) for a range of mutant selection coefficients, s_m, and mutation rates, μ.

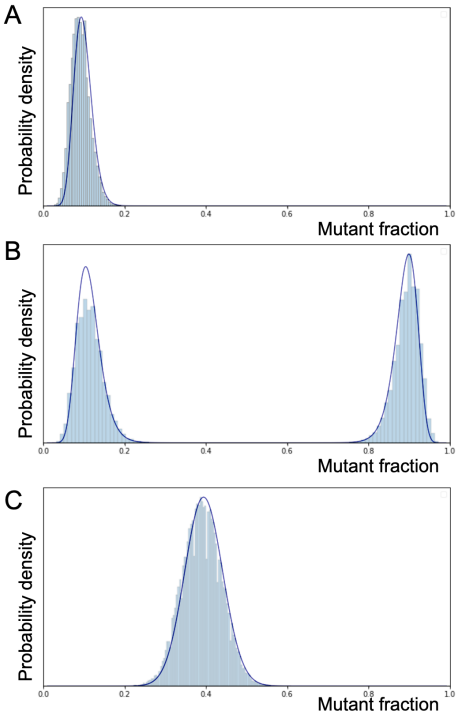

Figure S4. Fokker-Planck description of probability density holds under a range of interaction parameters. Each example represents the analytical (dark blue line, overlay) and a histogram of 100 sampled values of the mutant fraction from 500 independent simulations. **(A)** $s_m = -0.05$, $\alpha_{wm} = -0.05$, $\alpha_{wm} = -0.05$, $\mu = -0.01$, $N = 1000$. **(B)** $s_m = -0.05$, $\alpha_{wm} = -0.05$, $\alpha_{wm} = -0.05$, $\mu = -0.01$, $N = 1000$. **(C)** $s_m = -0.05$, $\alpha_{wm} = -0.05$, $\alpha_{wm} = -0.05$, $\mu = -0.01$, $N = 1000$. Further simulations of different mutation rates and different intrinsic selection coefficients.

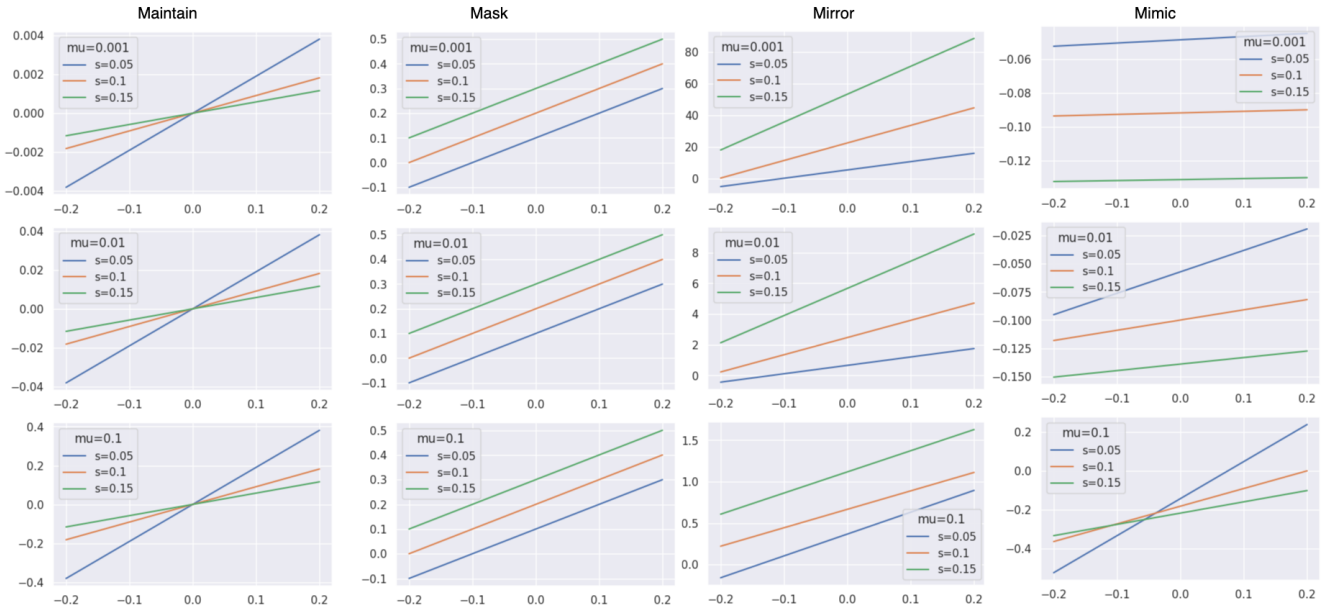

Figure S5. Relationship between interaction coefficients. The relationships between α_{mw} and α_{wm} as defined analytically in the main text. Functions for maintenance, masking, mirroring, and mimicry are plotted for three fixed mutation rates and varying intrinsic selection coefficients.

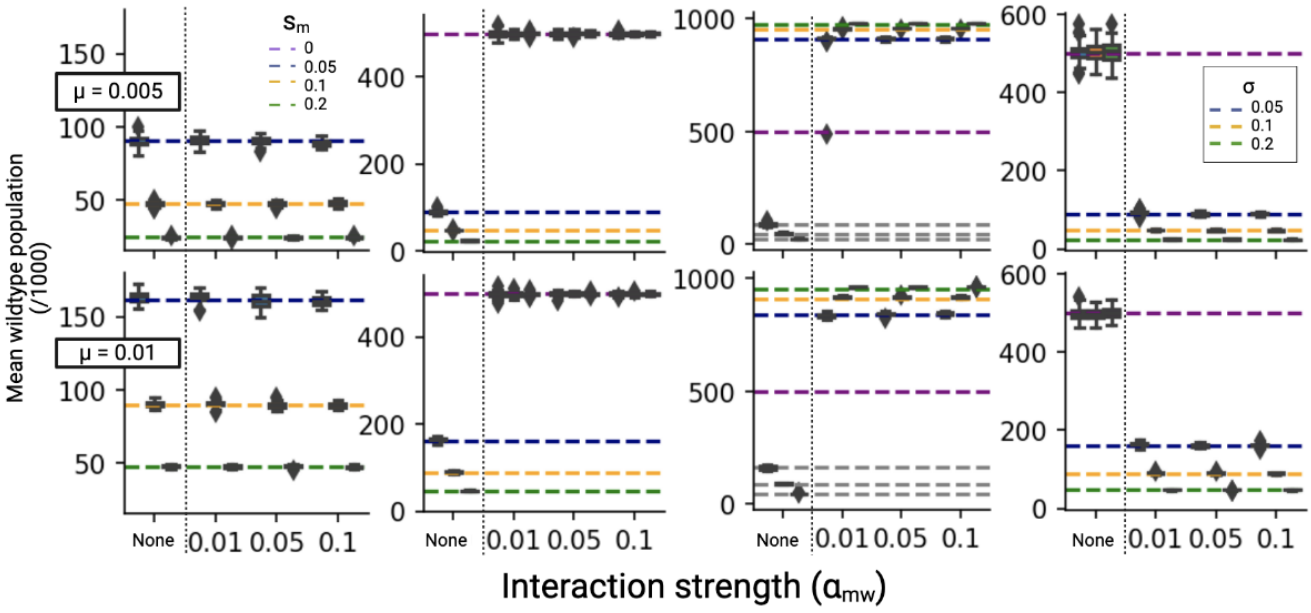

Figure S6. Masking, mimicry, maintenance, and mirroring predictions hold under parameter alteration. Further simulations of maintenance, masking, mirroring, and mimicry for different mutation rates and different intrinsic selection coefficients.

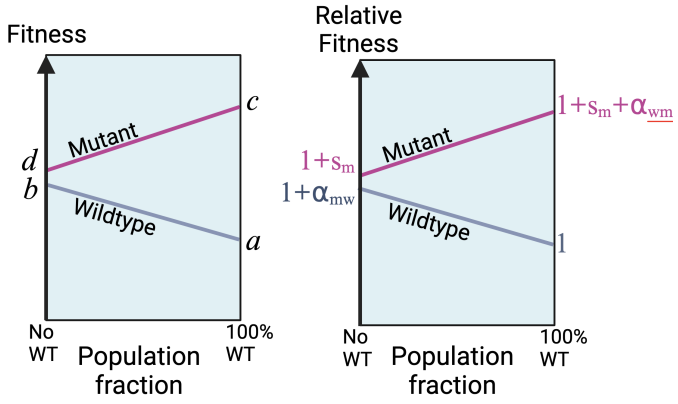

Figure S7. Illustration of how experimental game assay fitness-frequency plot can be rewritten in terms of the intrinsic and ecological interaction terms. (Left) The payoff matrix consists of the values of the four intersections of the frequency-fitness lines with the axes. While the 100% WT or mutant fractions can be directly measured, the infinitesimally small $\rightarrow$ 0% growth rate of the minority population is impossible to measure directly and must be inferred using regression and assumptions (of linearity or otherwise) from the other values. **(Right)** The equivalence of the intersections in terms of the modified payoff matrix is shown where the growth rates are normalized to the wild type. In the traditional game plot, the differences between the intersections are plotted, the two resultant values are functions of 3 variables and thus form a many-to-one mapping.

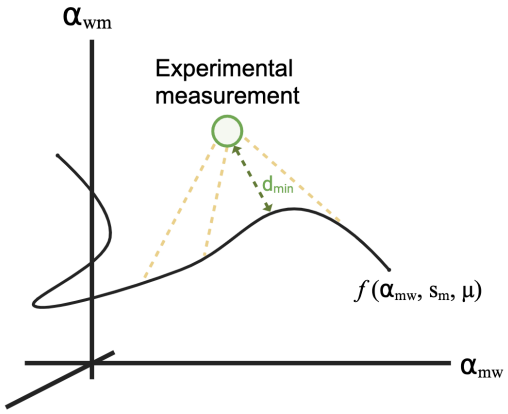

Figure S8. Illustration of Euclidean distance of the experimental data points from a theoretical regime. Distance $d_{\min}$ is calculated via numerical optimization (Python) to find the minimum distance between the point representing the experimental result $(\alpha_{wm}, \alpha_{mw}, s, \mu)$ and all points constrained to the specific manifolds $(\alpha_{wm} = f(\alpha_{mw}, s, \mu))$ that represent the theoretical conditions of masking, maintenance, and mirroring.

Supplemental Tables

Table S1. Additional details of the published experiments used to derive payoff matrices

Author	Year	System	Variable	Payoff matrices	Data Type
Vulic and Kolter [2]	2001	Bacteria	*Escheria coli* WT and GASP mutant	1	Growth-Frequency Plot
Li et al. [3]	2015	Bacteria	*Curvibacter* sp. (AEP1.3) and *Duganella* sp. (C1.2)	1	Growth-Frequency Plot
Kaznatcheev et al. [1]	2019	Cancer	NSCLC Cell Lines Drug+Fibroblasts	4	Payoff matrix
Adamowicz et al. [4]	2020	Bacteria	*Escheria coli*, *Salmonella enterica* *mdoG* and *mdoH* gene mutants	3	Growth-Frequency Plot
Cai et al. [5]	2020	In-silico	Metabolic simulation	1	Payoff
Faroukkian et al. [6]	2020	Cancer	NSCLC Cell lines Mutation, Drug	5	Payoff
Deris et al. [7]	2023	Cancer	Breast Cancer PDX Biological Replicates	10	Payoff
Maltas et al. [8]	2024	Cancer	NSCLC Cell Line Mutation, Drug	4	Payoff

References

1. Kaznatcheev, A., Peacock, J., Basanta, D., Marusyk, A. & Scott, J. G. Fibroblasts and alectinib switch the evolutionary games played by non-small cell lung cancer. *Nat. ecology & evolution* **3**, 450–456 (2019).

2. Vulić, M. & Kolter, R. Evolutionary cheating in escherichia coli stationary phase cultures. *Genetics* **158**, 519–526 (2001).

3. Li, X.-Y. *et al.* Which games are growing bacterial populations playing? *J. The Royal Soc. Interface* **12**, 20150121 (2015).

4. Adamowicz, E. M., Muza, M., Chacón, J. M. & Harcombe, W. R. Cross-feeding modulates the rate and mechanism of antibiotic resistance evolution in a model microbial community of escherichia coli and salmonella enterica. *PLoS pathogens* **16**, e1008700 (2020).

5. Cai, J., Tan, T. & Chan, S. H. Predicting nash equilibria for microbial metabolic interactions. *Bioinformatics* **36**, 5649–5655 (2020).

6. Farrokhian, N. *et al.* Measuring competitive exclusion in non–small cell lung cancer. *Sci. Adv.* **8**, eabm7212 (2022).

7. Deris, A. & Sohrabi-Haghighat, M. Analysis of cancerous tumor growth by the competitive model based on the evolutionary game theory. *Int. J. Nonlinear Analysis Appl.* **14**, 1903–1910 (2023).

8. Maltas, J. *et al.* Frequency-dependent ecological interactions increase the prevalence, and shape the distribution, of pre-existing drug resistance (in press). *PRX Life* DOI: 10.1101/2023.03.16.533001 (2024).

Table S2. Payoff values and equivalent selection and interaction terms extracted from papers

	Paper	a	b	c	d	s	α_{wm}	α_{mw}
0	Kaznatcheev2019	2.6	3.5	3.1	3.0	0.1538	0.3462	0.0385
1	Kaznatcheev2019	2.5	2.4	4.0	2.7	0.08	-0.04	0.52
2	Kaznatcheev2019	0.5	-0.4	3.8	2.4	3.8	-1.8	2.8
3	Kaznatcheev2019	2.3	4.3	-1.3	-1.0	-1.4348	0.8696	-0.1304
4	Maltas2024	1.0	0.97	0.97	0.84	-0.16	-0.03	0.13
5	Maltas2024	1.03	0.99	1.01	0.93	-0.0971	-0.0388	0.0777
6	Maltas2024	1.0	1.02	0.95	0.88	-0.12	0.02	0.07
7	Maltas2024	1.01	1.01	0.98	0.9	-0.1089	0.0	0.0792
8	Farrokhian2022	0.9963	1.004	0.975	0.7517	-0.2455	0.0077	0.2241
9	Farrokhian2022	0.47	0.42	0.83	0.7	0.4894	-0.1064	0.2766
10	Farrokhian2022	0.377	-0.01	0.86	0.714	0.8939	-1.01	0.3873
11	Farrokhian2022	0.37	-0.43	0.93	0.728	0.9676	-2.1622	0.5459
12	Farrokhian2022	0.33	-0.59	1.12	0.789	1.3909	-2.7879	1.003
13	VulicKolter2001	1.0	0.2	1.1	0.5	-0.5	-0.8	0.6
14	VulicKolter2001	0.5	1.1	0.2	1.0	1.0	1.2	-1.6
15	CaiChan2020	1.18	1.09	1.42	1.34	0.1356	-0.0763	0.0678
17	Li2015	0.1774	0.1284	0.13895	0.08	-0.549	-0.2762	0.3323
18	Deris2023	1.0	0.0	1.72	0.24	-0.76	-1.0	1.48
19	Deris2023	0.5	0.0	1.06	0.1	-0.8	-1.0	1.92
20	Deris2023	1.0	0.0	1.6	0.87	-0.13	-1.0	0.73
21	Deris2023	1.2	0.0	1.8	0.7	-0.4167	-1.0	0.9167
22	Deris2023	1.0	0.0	1.65	0.5	-0.5	-1.0	1.15
23	Deris2023	3.2	0.0	5.0	0.5	-0.8438	-1.0	1.4063
24	Deris2023	1.0	0.0	1.8	0.5	-0.5	-1.0	1.3
25	Deris2023	1.0	0.0	1.65	0.5	-0.5	-1.0	1.15
26	Deris2023	1.0	0.0	1.58	0.8	-0.2	-1.0	0.78
27	Deris2023	6.0	0.0	8.3	0.4	-0.9333	-1.0	1.3167
29	Adamowicz2020	0.89	0.37	0.15	0.61	-0.3146	-0.5843	-0.5169
30	Adamowicz2020	0.45	0.4	0.43	0.6	0.3333	-0.1111	-0.3778
31	Adamowicz2020	0.64	0.39	0.41	0.29	-0.5469	-0.3906	0.1875